Materials Horizons

ROYAL SOCIETY OF CHEMISTRY

COMMUNICATION

View Article Online
View Journal | View Issue

Open Access Article. Published on 11 April 2024. Downloaded on 2/21/2026 12:13:01 PM.
This article is licensed under a Creative Commons Attribution-NonCommercial 3.0 Unported Licence.

Check for updates

Cite this: *Mater. Horiz.*, 2024, **11**, 3076

Received 7th February 2024,
Accepted 11th April 2024

DOI: 10.1039/d4mh00142g

rsc.li/materials-horizons

Aggregation-induced emission organic metal halide complex for X-ray scintillation†

Tunde Blessed Shonde,[a] He Liu,[a] Oluwadara Joshua Olasupo,[a] Alexander Bouchard,[a] Sara Bouchard,[a] Annaliese Franklin,[a] Xinsong Lin,[a] Luis M. Stand[cd] and Biwu Ma*[ab]

The expanding applications of X-ray scintillation across various areas, from healthcare to security detection call for the development of new-generation scintillators that offer enhanced sensitivity, efficiency, and versatility. Here, we report for the first time the use of organic metal halide complexes with aggregation-induced emission (AIE) for X-ray scintillation, which can be facilely synthesized and processed in the solution phase. By reacting an AIE organic molecule, 4-(4-(diphenylamino) phenyl)-1-(propyl)-pyridinium (TPA-PD) with zinc chloride ($ZnCl_2$) in solution at room temperature, an organic metal halide complex, $(TPA\text{-}PD)_2ZnCl_2$, is produced with a high synthetic yield of 87%. Optical and radioluminescence characterizations find that $(TPA\text{-}PD)_2ZnCl_2$ exhibits bluish-green photoluminescence and radioluminescence peaked at around 450 nm, with a photoluminescence quantum efficiency (PLQE) of 65%, and an absolute light yield of 13 423 Photon per MeV. Moreover, short photoluminescence and radioluminescence decay lifetimes are recorded at 1.81 ns and 5.24 ns, respectively. For X-ray scintillation, an excellent response dose–response linearity and a low limit of detection of 80.23 $nGy_{air}\ S^{-1}$ are obtained for $(TPA\text{-}PD)_2ZnCl_2$. By taking advantage of the high X-ray absorption of metal halides and fast radioluminescence of AIE molecules, our design of covalently bonded organic metal halide complexes opens up new opportunities for the development of high-performance solution-processable scintillators.

New concepts

Scintillators, converting high-energy radiation to UV-visible light, are widely used in fields from medical diagnosis to space exploration. Despite various materials like inorganic, organic, and plastic scintillators, none meets all desired features: high X-ray absorption, rapid responsivity, exceptional processability, cost-effectiveness, and low toxicity. Organic metal complexes, bonding organic ligands to metal species, offer potential advantages by combining organic and inorganic unit merits. Yet, this class of materials remain largely unexplored in scintillation applications. Here, we introduce, for the first time, the use of organic metal halide complexes with aggregation-induced emission (AIE) for X-ray scintillation. By reacting an AIE molecule, 4-(4-(diphenylamino) phenyl)-1-(propyl)-pyridinium (TPA-PD), with zinc chloride ($ZnCl_2$) in solution at room temperature, an organic metal halide complex, $(TPA\text{-}PD)_2ZnCl_2$, is produced with a high yield of 87%. This complex exhibits bluish-green photoluminescence and radioluminescence centered at 450 nm, with a photoluminescence quantum efficiency (PLQE) of 65% and an absolute light yield of 13 423 Photon per MeV. Additionally, it demonstrates short photoluminescence and radioluminescence decay lifetimes of 1.81 ns and 5.24 ns, respectively. Leveraging the high X-ray absorption of metal halides and the fast radioluminescence of AIE molecules, our covalently bonded organic metal halide complexes pave the way for the development of high-performance solution-processable scintillators.

Introduction

X-ray and other forms of high-energy radiation are of great importance in numerous fields, including medical diagnosis and treatment, space exploration, non-destructive product inspection, pulsar navigation, and so on.[1–9] Scintillators, capable of converting these ionizing radiations to ultraviolet (UV)-visible light, find widespread use in radiation detection and imaging.[10–14] To date, the most commonly used scintillators are based on inorganic crystals, *e.g.* $PbWO_4$, $Bi_4Ge_3O_{12}$, thallium doped CsI (CsI:Tl), and cerium doped $YAlO_3$ ($YAlO_3$:Ce).[14] While these scintillation materials satisfy certain application requirements, many issues and challenges remain to be addressed, including brittle nature, hygroscopicity, time-consuming high-temperature synthesis, and long decay lifetimes, to name a few.[15,16,17] Organic and plastic scintillators such as anthracene, stilbene, polyvinyl toluene, and polystyrene offer many unique advantages like flexibility and low cost, with short decay lifetimes, making them valuable alternatives to inorganic scintillators in certain applications.[12,18–20] However,

[a] *Department of Chemistry and Biochemistry, Florida State University, Tallahassee, FL, 32306, USA. E-mail: bma@fsu.edu*
[b] *Materials Science and Engineering Program, Florida State University, Tallahassee, FL 32306, USA*
[c] *Department of Nuclear Engineering, University of Tennessee, Knoxville, TN 37996, USA*
[d] *Scintillation Materials Research Canter, University of Tennessee, Knoxville, TN 37996, USA*

† Electronic supplementary information (ESI) available. CCDC 2267984. For ESI and crystallographic data in CIF or other electronic format see DOI: https://doi.org/10.1039/d4mh00142g

This journal is © The Royal Society of Chemistry 2024

Open Access Article. Published on 11 April 2024. Downloaded on 2/21/2026 12:13:01 PM.
This article is licensed under a Creative Commons Attribution-NonCommercial 3.0 Unported Licence.

their low radiation hardness, poor thermal stability, and most importantly, their weak radiation attenuation and low scintillation light yield prevent a widespread use of these predominately carbon-based scintillators.[1,12] Developing new types of scintillation materials that combine the advantages of inorganic and organic scintillators has been one of the major focuses for the researchers In the field.[1,19,21]

To overcome the low X-ray absorption capability of organic scintillators, molecular sensitization of luminescent organic components by high-Z components has been established as an effective approach in various types of material systems. Physically blending luminescent organic molecules with high-Z oxides, metal complexes, and halide perovskites has been reported to enhance the X-ray absorption of hybrid composite systems.[4,19,22] However, the non-uniformity of the blends, as well as the inferior energy/charge transfer between high-Z components and organic molecules, limit the overall performance. Recently, chemically bonding organic units with high-Z components has produced scintillation materials with much better performance than those of blends. For example, efficient X-ray scintillation based on high X-ray absorbing Pb(II) and interconnected luminescent naphthalene organic ligand motifs was reported by J. Lu *et al.*[23] In 2022, J. Perego *et al.* reported fluorescent conjugated acene ligands, co-assembled by zirconium oxy-hydroxyl clusters for scintillation application.[24] More recently, our group reported for the first time ionically bonded zero-dimensional (0D) organic metal halide hybrid scintillators with molecular sensitization, in which high Z metal halides act as X-ray sensitizers and AIE organic cations as emitters.[1] Significantly improved X-ray absorption and radioluminescence have been reported for these organic metal halide hybrid scintillators as compared to pure organic molecules. However, the ionic nature of organic metal halide hybrids may limit their processability.

Organic metal complexes, in which organic ligands are covalently bonded to metal ions, have been investigated extensively during the past few decades with a wide range of applications, from catalysis to electronics, photonics, and medicine.[25] However, their potential as scintillators has been largely underexplored, with very few cerium and lanthanide-based organic metal complexes reported to exhibit low light yields.[26,27] Also, the presence of heavy atoms in these organic metal complexes often leads to long-lived phosphorescent emissions, which is undesirable for dynamic X-ray imaging, high-energy particle physics research, and many other applications. Therefore, further the exploration of organic metal complexes is necessary to develop efficient, rapid, and solution-processable scintillators.

Here we report an organic metal halide complex scintillator with high absolute light yield and fast radioluminescence, which could be facilely prepared by reacting an AIE organic molecule, 4-(4-(diphenylamino) phenyl)-1-(propyl)-pyridinium (TPA-PD) with low cost and non-toxic zinc chloride ($ZnCl_2$) in solution at room temperature. In this covalently bonded organic metal halide complex, ($(TPA\text{-}PD)_2ZnCl_2$), the appropriate distance between the aggregative-induced emissive (AIE) active TPA-PD moieties and metal halides ($ZnCl_2$) enables efficient molecular sensitization, with $ZnCl_2$ harvesting high energy radiation and subsequently realizing charge transfer to the organic units. Additionally, zinc chloride modulates the intra-ligand emission by increasing molecular rigidity and suppressing non-radiative decays, leading to enhanced radioluminescence. $(TPA\text{-}PD)_2ZnCl_2$ is found to exhibit an absolute light yield of 13 423 Photon per MeV, which is more than 4.5 times higher than that of the pure AIE molecule TPA-PD (2980 Photon per MeV) and twice of that of a commercially available zinc complex bis[2-(2-benzothiazolyl)phenolato]-zinc(II) (BBPZn) (6249 Photon per MeV). $(TPA\text{-}PD)_2ZnCl_2$ also exhibits fast photoluminescence and radioluminescence decays, with lifetimes in nanoseconds, excellent dose linearity, and a low limit of detection of 80.23 $nGy_{air}\ S^{-1}$.

Results and discussion

The synthetic procedures for the preparation of *N*,*N*-diphenyl-4-(pyridine-4-yl)aniline ($C_{23}H_{18}N_2$, TPA-PD) and *N*,*N*-diphenyl-4-(pyridine-4-yl)aniline zinc(II) chloride ($C_{46}H_{36}N_4ZnCl_2$, $(TPA\text{-}PD)_2ZnCl_2$) are depicted in Fig. 1a and b. TPA-PD was synthesized following a literature-reported procedure, in which nitrogen-based π-deficient pyridine was coupled to electron-rich triphenylamine through palladium-catalyzed Suzuki cross-coupling.[28,29] $(TPA\text{-}PD)_2ZnCl_2$ single crystals were prepared by solvent layering of acetonitrile on the precursor solution containing TPA-PD and $ZnCl_2$ in a 2 : 1 molar ratio. Detailed descriptions of synthesis, purification, and purity analysis can be found in the method section. Fig. 1c and d show TPA-PD and $(TPA\text{-}PD)_2ZnCl_2$ under ambient light, with TPA-PD and $(TPA\text{-}PD)_2ZnCl_2$ displaying white and yellowish-white color, respectively.

The composition and structure of TPA-PD and $(TPA\text{-}PD)_2ZnCl_2$ are fully characterized by elemental analysis, ^1H NMR (Fig. S1 and S2, ESI†), powder (Fig. S3, ESI†), and single crystal X-ray diffraction. The single crystal structures and molecular packings of TPA-

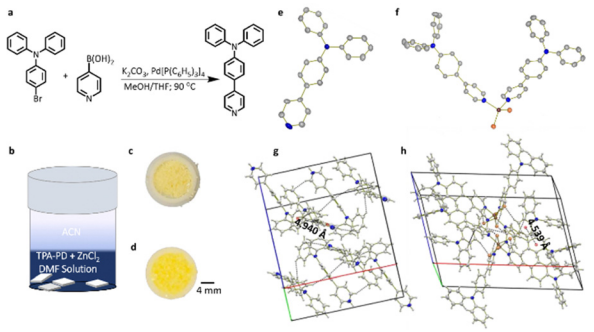

Fig. 1 (a) Synthetic scheme for the preparation of TPA-PD; (b) synthetic scheme for the preparation of $(TPA\text{-}PD)_2ZnCl_2$; (c) image of TPA-PD under daylight; (d) image of $(TPA\text{-}PD)_2ZnCl_2$ under daylight; (e) molecular structure of TPA-PD; (f) molecular structure of $(TPA\text{-}PD)_2ZnCl_2$; (g) molecular packing for TPA-PD; (h) molecular packing for $(TPA\text{-}PD)_2ZnCl_2$; grey color represents carbon; blue, nitrogen; light orange; light gray, hydrogen. The orange-to-orange distance shows the π···π distances. Ellipsoids are drawn at their 50% probability level.

Open Access Article. Published on 11 April 2024. Downloaded on 2/21/2026 12:13:01 PM.
This article is licensed under a Creative Commons Attribution-NonCommercial 3.0 Unported Licence.

PD and $(TPA\text{-}PD)_2ZnCl_2$ are shown in Fig. 1g and h. Detailed crystallographic information can be found in Tables S1 and S2 (ESI†). Selected angles and bonds are given in Table S2 (ESI†). It is found that the Zn core is coordinated with two TPA-PD moieties and two chlorides in a distorted tetrahedral geometry, in which the average Zn–N and Zn–Cl distances are 2.044 Å and 2.235 Å, respectively. $(TPA\text{-}PD)_2ZnCl_2$ crystallizes into a monoclinic $p21/c$ space group with a unit cell volume of 3804.6 $Å^3$ and density, 1.364 g cm^{-3}. TPA-PD crystallizes into $C2/c$ space group and has a cell volume of 3342.4 $Å^3$ and a density of 1.281 g cm^{-3}. Both TPA-PD and $(TPA\text{-}PD)_2ZnCl_2$ essentially show similar molecular packings with the shortest $\pi\cdots\pi$ distance of 4.940 Å in TPA-PD and 4.539 Å in $(TPA\text{-}PD)_2ZnCl_2$, suggesting little-to-no $\pi\cdots\pi$ interactions. Additionally, there is a close CH–π proximity in both molecules, with shortest distances of 2.820 Å and 2.861 Å for TPA-PD and $(TPAPD)_2ZnCl_2$, respectively, which hinders the intermolecular rotation. To assess the thermal properties of these compounds, thermogravimetric analysis (TGA) and differential scanning calorimetry (DSC) were performed with results shown in Fig. S4 (ESI†). Onset weight loss is observed for TPA-PD and $(TPA\text{-}PD)_2ZnCl_2$ at 300 °C and 326 °C, respectively. The thermogram from the DSC reveals the melting point peak apex of TPA-PD and $(TPA\text{-}PD)_2ZnCl_2$ to be 145 °C and 267 °C, with full width at half maximum (FWHM) of ∼7 °C and 5 °C, respectively. The small FWHM (<10 K) indicates the materials are pure crystalline solids. The commercially available organic zinc complex, BBPZn has an onset weight loss and melting temperature of 414 °C and 303 °C, respectively.

The photophysical properties of crystal samples of TPA-PD and $(TPA\text{-}PD)_2ZnCl_2$ have been characterized with their absorption, emission, and decay dynamics shown in Fig. 2. Both TPA-PD and $(TPA\text{-}PD)_2ZnCl_2$ are found to possess similar broad absorption bands with three peaks, corresponding to the transitions occurring at the triphenylamine and pyridine moieties in the organic ligands. With photoexcitation at 365 nm, TPA-PD and $(TPA\text{-}PD)_2ZnCl_2$ exhibit deep blue and greenish-blue emissions, respectively. Their emission spectra show peaks at 398 nm and 448 nm with full width at half maximums (FWHMs) of 47 nm and 67 nm, respectively. These featureless emissions are attributed to the intramolecular charge transfer (ICT) between the triphenylamine and pyridine moieties, a well-known phenomenon in push–pull chromophore systems.[30] The slightly redshifted absorption and emission spectra of $(TPA\text{-}PD)_2ZnCl_2$ as compared to those of TPA-PD are believed to be caused by the perturbation of the ICT states with the binding of the Zn metal,[31–33] although the closed d^{10} shell configuration leads to its non-participatory role in the emission. The reference organic zinc complex, BBPZn displays narrower featureless absorption and emission spectra with peaks at 244 nm and 475 nm. The insets of Fig. 2a show the images of the three compounds under a 365 nm UV lamp excitation. The PLQEs of these compounds in solid state were determined to be 27%, 65%, and 42% for TPA-PD, $(TPA\text{-}PD)_2ZnCl_2$, and BBPZn, respectively (Fig. S5, ESI†). The higher PLQE of $(TPA\text{-}PD)_2ZnCl_2$ than that of TPA-PD is likely attributed to the increased molecular rigidity with suppression

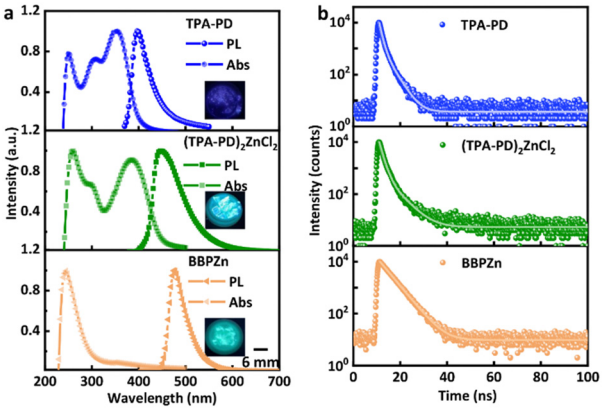

Fig. 2 (a) Absorbance and emission spectra of TPA-PD, $(TPA\text{-}PD)_2ZnCl_2$, and BBPZn; insets show the images of TPA-PD, $(TPA\text{-}PD)_2ZnCl_2$, and BBPZn under a 365 nm UV lamp excitation; (b) photoluminescence decay kinetics of TPA-PD, $(TPA\text{-}PD)_2ZnCl_2$, and BBPZn.

of nonradiative decays. The photoluminescence decay kinetics of these compounds were investigated using time-resolved photoluminescence (TRPL) spectroscopy. As shown in Fig. 2b and Table S3 (ESI†), both TPA-PD and $(TPA\text{-}PD)_2ZnCl_2$ show bi-exponential decays with average lifetimes of 1.59 ns and 1.81 ns, respectively. The similar decay kinetics are not surprising as TPA-PD and $(TPA\text{-}PD)_2ZnCl_2$ are both AIE compounds with emissions from the same ICT state. On the other hand, BBPZn shows a mono-exponential decay, with a lifetime of 4.00 ns.

The potential of the three compounds, TPA-PD, $(TPA\text{-}PD)_2ZnCl_2$, and BBPZn, for X-ray scintillation has been evaluated. First, the effective Z values and linear absorption coefficients in term of photon energy were determined for all the three compounds, as shown in Fig. 3a and b. Across the studied photon energy range, the effective Z of $(TPA\text{-}PD)_2ZnCl_2$ is much higher than that of TPA-PD, but slightly lower than that of BBPZn. The theoretical linear absorption coefficients of $(TPA\text{-}PD)_2ZnCl_2$ and BBPZn are similar, which are much higher than that of TPA-PD. Fig. S6a (ESI†) shows the mass absorption coefficient *vs.* photon energy plot. Fig. S6b and c (ESI†) display the X-ray attenuation efficiency *vs.* thickness at 39.2 KeV and 10.3 KeV X-ray photon, respectively. Clearly at 0.1 cm thickness, $(TPA\text{-}PD)_2ZnCl_2$ and BBPZn can attenuate 100% of 10.3 KeV, while more than 0.5 cm of TPA-PD is required to attenuate similarly. These results clearly show that incorporating high Z atoms into hydrocarbon based organic molecules improves X-ray absorption. The radioluminescence (RL) properties of the three compounds were characterized. As shown in the inset of Fig. 3c, TPA-PD, $(TPA\text{-}PD)_2ZnCl_2$ and BBPZn, exhibit visible radioluminescence, with excitation using an X-ray generator (Moxtek Mini tube, tungsten target, 4 W), similar to the photoluminescence under UV excitation. The radioluminescence spectra of the three compounds were recorded using a fluorescence spectrophotometer coupled with the X-ray generator, as shown in Fig. 3c. Similar to the photoluminescence spectra, the radioluminescence spectra are featureless with peaks at 403 nm, 447 nm, 487 nm for TPA-PD, $(TPA\text{-}PD)_2ZnCl_2$, and BBPZn, respectively. Using a time-correlated single photon

Open Access Article. Published on 11 April 2024. Downloaded on 2/21/2026 12:13:01 PM.
This article is licensed under a Creative Commons Attribution-NonCommercial 3.0 Unported Licence.

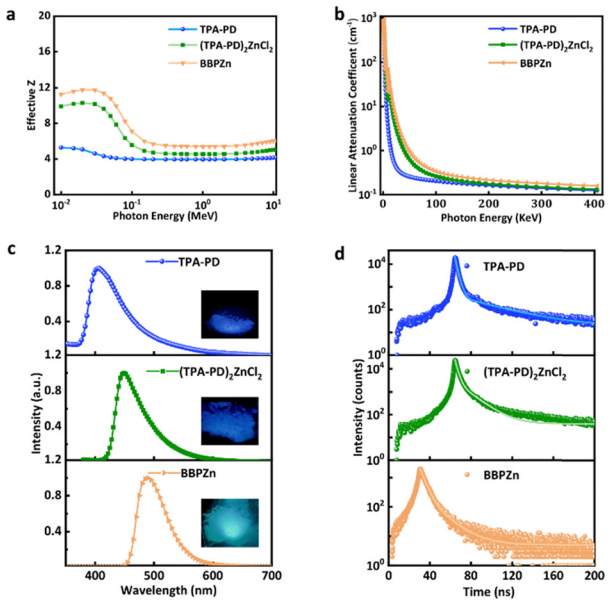

Fig. 3 (a) Computed effective Z *vs.* photon energy plot of TPA-PD, (TPA-PD)$_2$ZnCl$_2$, and BBPZn; (b) computed linear attenuation coefficient *vs.* photon energy plot of TPA-PD, (TPA-PD)$_2$ZnCl$_2$, and BBPZn; (c) radioluminescence spectra of TPA-PD, (TPA-PD)$_2$ZnCl$_2$, and BBPZn; (d) radioluminescence decay kinetics of TPA-PD, (TPA-PD)$_2$ZnCl$_2$, and BBPZn.

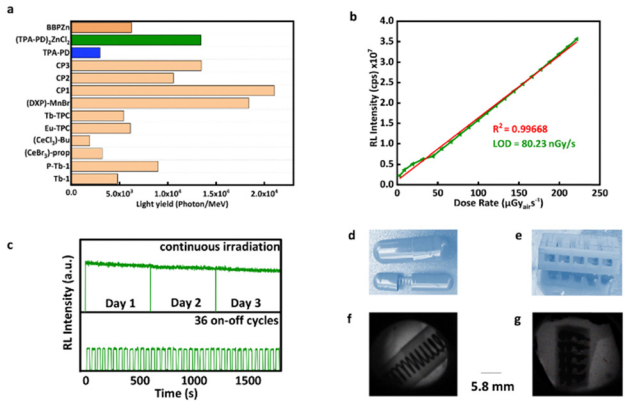

Fig. 4 (a) Comparison of light yield of reported scintillators based on metal organic complex; (b) dose–response linearity measurement of (TPA-PD)$_2$ZnCl$_2$; (c) the emission radio-stability at 448 nm for the (TPA-PD)$_2$ZnCl$_2$ *versus* continuous irradiation (top) and repeated on–off cycles of X-rays (bottom) at a dose rate of 221.39 μGy s^{-1}; (d) an encapsulated metallic spring; (e) an electronic circuit; (f) the X-ray image of the encapsulated spring; (g) the X-ray image of electronic circuit.

counting technique (^{137}Cs excitation source, 662 keV), the radioluminescence decay kinetics were studied for the three compounds, exhibiting biexponential decays with average lifetimes of 9.86 ns, 5.24 ns, and 6.78 ns, respectively (Fig. 3d, see experimental details).

The absolute scintillation light yields of TPA-PD, (TPA-PD)$_2$ZnCl$_2$, and BBPZn were determined using the single photoelectron technique with a factory-measured quantum efficiency R2059 Photomultiplier Tube (PMT) (Fig. S7, see experimental details, ESI†). (TPA-PD)$_2$ZnCl$_2$ was found to have an absolute light yield of 13 423 Photon per MeV, which is significantly higher than those of TPA-PD (2 980 Photon per MeV) and BBPZn (6 249 Photon per MeV). Indeed, (TPA-PD)$_2$ZnCl$_2$ has one of the highest absolute light yields among all the reported organic metal complex scintillators (Fig. 4a and Table S4, ESI†).[26,27,34–36] With short radioluminescence decay lifetime and high absolute light yield, (TPA-PD)$_2$ZnCl$_2$ is highly promising for certain applications that require fast responses, such as X-ray dynamic imaging and high-energy physics experiments. To measure the thickness-dependent RL, TPA-PD, (TPA-PD)$_2$ZnCl$_2$, and BBPZn were made into pellets (0.5–5 mm) with hydraulic press of 1 metric ton load for 30 seconds. Powder X-ray diffraction spectra of the crystals and pellets show similar results (Fig. S8, ESI†), suggesting that phase and structural integrity are maintained. Steady increase of RL responses upon the increasing of pellet thickness can clearly be seen until 3.00 mm (Fig. S9a and b, ESI†). BBPZn shows RL steady increase up to 3.50 mm (Fig. S9c, ESI†). The dose linearity was determined by irradiating these materials with X-ray dose rate in a descending dose rate order, from 3.08 to 221.39 to 3.08 μGy s^{-1}. As shown in Fig. 4b and Fig. S10 and S11 (ESI†), all the samples show excellent response linearities to dose rates. The limit of detection (LOD), an important performance metric, was determined to be 538.04 nGy$_{air}$ S^{-1} for TPA-PD, 80.23 nGy$_{air}$ S^{-1} for (TPA-PD)$_2$ZnCl$_2$, and 15.56 nGy$_{air}$ S^{-1} for (BBPZn), which are significantly lower than the standard dose for X-ray medical diagnostics (5.5 μGy$_{air}$S^{-1}). The radio-stability was investigated with results shown in Fig. 4c and Fig. S12 (ESI†). Under continuous high dose rate (221.39 μGy$_{air}$S^{-1}) irradiation for 30 mins, the RL intensities of TPA-PD and (TPA-PD)$_2$ZnCl$_2$ remain at 95%, and BBPZn at 94% of their initial RL intensities, which are comparable to commercially available plastic scintillators.[37] Moreover, the RL intensity of (TPA-PD)$_2$ZnCl$_2$ is stable under repeated X-ray excitation with 36 cycles on and off, as shown in Fig. 4c.

Given the remarkable RL properties of (TPA-PD)$_2$ZnCl$_2$, X-ray imaging capability was tested on a 260 μm film of (TPA-PD)$_2$ZnCl$_2$ (60 wt%)-poly methyl methacrylate (PMMA) composite (Fig. S13a, ESI†). The composite was mounted on a lab-built X-ray imaging setup (Fig. S13b, ESI†), comprising of X-ray source, sample holder for objects (Fig. 4d and e), light ray deflector, and a digital camera. Fig. 4f and g show imaging capability of the composite under 221.39 μGy s^{-1}. The images obtained reveal the internal structure of the visualized objects with great clarity. Furthermore, Fig. S14 (ESI†) displays the X-ray images produced under various lower X-ray dose rates, elucidating the (TPA-PD)$_2$ZnCl$_2$-PMMA composite's ability to consistently provide clear X-ray images even at low X-ray dose rates. This demonstrates the significant potential of the (TPA-PD)$_2$ZnCl$_2$ for non-destructive testing.

Conclusions

In conclusion, we have developed an efficient molecular scintillator based on aggregate induced emission (AIE) organic zinc halide complex (TPA-PD)$_2$ZnCl$_2$. This covalently bonded organic metal

Open Access Article. Published on 11 April 2024. Downloaded on 2/21/2026 12:13:01 PM.
This article is licensed under a Creative Commons Attribution-NonCommercial 3.0 Unported Licence.

halide complex with molecular sensitization not only exhibits good X-ray absorption due to the presence of high Z metal halides, but also possesses efficient and fast radioluminescence in solid state, thanks to its AIE nature. The high absolute light yield of 13 423 Photon per MeV, short radioluminescence decay lifetime of 5.24 ns, and low detection limit of 80.23 nGy_{air} S^{-1} are among the best values achieved to date for molecular scintillators. This work provides a promising design strategy for the development of high-performance and low-cost scintillators based on earth-abundant organic metal complexes, and significantly expands the range of low-cost, solution-processable scintillators.

Conflicts of interest

T. B. S. and B. M. have filed a patent application ''Organic Metal Complex Scintillators and Methods of Making the Same'' to the United States Patent and Trademark Office on February 22, 2024, as Serial No. 63/556,540.

Acknowledgements

The authors acknowledge the funding support from the National Science Foundation (NSF) (DMR-2204466) and the Florida State University GAP Commercialization Investment Program. This work made use of the Rigaku Synergy-S single-crystal X-ray diffractometer, which was acquired through the NSF MRI program (CHE-1828362). We also thank NSF Research Experiences for Undergraduates (NSF-REU) Sites program (CHE-2150301).

Notes and references

1 T. B. Shonde, M. Chaaban, H. Liu, O. J. Olasupo, A. Ben-Akacha, F. G. Gonzalez, K. Julevich, X. Lin, J. S. Raaj Vellore Winfred, L. M. Stand, M. Zhuravleva and B. Ma, *Adv. Mater.*, 2023, **35**, 2301612.
2 L.-J. Xu, X. Lin, Q. He, M. Worku and B. Ma, *Nat. Commun.*, 2020, **11**, 4329.
3 Q. He, C. Zhou, L. Xu, S. Lee, X. Lin, J. Neu, M. Worku, M. Chaaban and B. Ma, *ACS Mater. Lett.*, 2020, **2**, 633–638.
4 T. B. Shonde, A. Mondal, H. Liu, M. Chabaan, A. Ben-Akacha, S. Lee, E. S. Knorr and B. Ma, *ACS Mater. Lett.*, 2022, **4**, 271–276.
5 V. Morad, Y. Shynkarenko, S. Yakunin, A. Brumberg, R. D. Schaller and M. V. Kovalenko, *J. Am. Chem. Soc.*, 2019, **141**, 9764–9768.
6 H. Yang, W. Xiang, X. Zhang, J. Wang, L. Xu and Z. Cheng, *J. Mater. Chem. C*, 2024, **12**, 438–442.
7 T. Yang, P. Wu, R. Chen, J. Ni, C. Xu, X. Liu, S. Wang and S. Liu, *J. Lumin.*, 2024, **269**, 120498.
8 S. A. Fateev, V. Y. Kozhevnikova, K. M. Kuznetsov, D. E. Belikova, V. N. Khrustalev, E. A. Goodilin and A. B. Tarasov, *Dalton Trans.*, 2024, **53**, 2722–2730.
9 N. Li, Y. Li, S. Xie, J. Wu, N. Liu, Y. Yu, Q. Lin, Y. Liu, S. Yang, G. Lian, Y. Fang, D. Yang, Z. Chen and X. Tao, *Angew. Chem., Int. Ed.*, 2023, **62**, e202302435.
10 C. Dujardin, E. Auffray, E. Bourret-Courchesne, P. Dorenbos, P. Lecoq, M. Nikl, A. N. Vasil'ev, A. Yoshikawa and R. Y. Zhu, *IEEE Trans. Nucl. Sci.*, 2018, **65**, 1977–1997.
11 F. Maddalena, L. Tjahjana, A. Xie, A. Arramel, S. Zeng, H. Wang, P. Coquet, W. Drozdowski, C. Dujardin, C. Dang and M. Birowosuto, *Crystals*, 2019, **9**, 88.
12 W. Ma, Y. Su, Q. Zhang, C. Deng, L. Pasquali, W. Zhu, Y. Tian, P. Ran, Z. Chen, G. Yang, G. Liang, T. Liu, H. Zhu, P. Huang, H. Zhong, K. Wang, S. Peng, J. Xia, H. Liu, X. Liu and Y. M. Yang, *Nat. Mater.*, 2021, **34**, 2204801.
13 S. R. Martins, S. T. Golafale, J. Bacsa, A. Steiner, C. W. Ingram, F. P. Doty, E. Auden and K. Hattar, *Dalton Trans.*, 2017, **46**, 491–500.
14 Q. Chen, J. Wu, X. Ou, B. Huang, J. Almutlaq, A. A. Zhumekenov, X. Guan, S. Han, L. Liang, Z. Yi, J. Li, X. Xie, Y. Wang, Y. Li, D. Fan, D. B. L. Teh, A. H. All, O. F. Mohammed, O. M. Wu Bakr, T. Bettinelli, M. H. Yang, W. Huang and X. Liu, *Nature*, 2018, **561**, 88–93.
15 W. Zhu, W. Ma, Y. Su, Z. Chen, X. Chen, Y. Ma, L. Bai, W. Xiao, T. Liu, H. Zhu, X. Liu, H. Liu, X. Liu and Y. M. Yang, *Light: Sci. Appl.*, 2020, **9**, 112.
16 V. V. Nagarkar, T. K. Gupta, S. R. Miller, Y. Klugerman, M. R. Squillante and G. Entine, *IEEE Trans. Nucl. Sci.*, 1998, **45**, 492–496.
17 S. Baccaro, K. Blaiek, F. de Notaristefani, P. Mally, J. A. Mares, R. Pani, R. Pellegrini and A. Soluri, *Nucl. Instr. Meth. Phys. Res. A*, 1995, 209–215.
18 J.-X. Wang, L. Gutiérrez-Arzaluz, X. Wang, M. Almalki, J. Yin, J. Czaban-Jóźwiak, O. Shekhah, Y. Zhang, O. M. Bakr, M. Eddaoudi and O. F. Mohammed, *Matter*, 2022, **5**, 253–265.
19 T. J. Hajagos, C. Liu, N. J. Cherepy and Q. Pei, *Adv. Mater.*, 2018, **30**, e1706956.
20 M. Koshimizu, *Jpn. J. Appl. Phys.*, 2022, **62**, 010503.
21 X. Liu, R. Li, X. Xu, Y. Jiang, W. Zhu, Y. Yao, F. Li, X. Tao, S. Liu, W. Huang and Q. Zhao, *Adv. Mater.*, 2023, **35**, e2206741.
22 M. Gandini, I. Villa, M. Beretta, C. Gotti, M. Imran, F. Carulli, E. Fantuzzi, M. Sassi, M. Zaffalon, C. Brofferio, L. Manna, L. Beverina, A. Vedda, M. Fasoli, L. Gironi and S. Brovelli, *Nat. Nanotechnol.*, 2020, **15**, 462–468.
23 J. Lu, X. H. Xin, Y. J. Lin, S. H. Wang, J. G. Xu, F. K. Zheng and G. C. Guo, *Dalton Trans.*, 2019, **48**, 1722–1731.
24 J. Perego, C. X. Bezuidenhout, I. Villa, F. Cova, R. Crapanzano, I. Frank, F. Pagano, N. Kratochwill, E. Auffray, S. Bracco, A. Vedda, C. Dujardin, P. E. Sozzani, F. Meinardi, A. Comotti and A. Monguzzi, *Nat. Commun.*, 2022, **13**, 3504.
25 F. Dumur, *Synth. Met.*, 2014, **195**, 241–251.
26 L. A. Boatner, J. S. Neal, J. O. Ramey, B. C. Chakoumakos, R. Custelcean, E. V. D. Van Loef, G. Markosyan and K. S. Shah, *Nucl. Instr. Meth. Phys. Res. A*, 2013, **703**, 138–144.
27 Z. Chen, D. Lu, H. Xie, X. Yang, Y. Li, C. Bao, L. Lei and S. Xu, *Adv. Opt. Mater.*, 2021, **10**, 2102074.
28 Y. Ma, Z. Zhuang, L. Xing, J. Li, Z. Yang, S. Ji, R. Hu, Z. Zhao, Y. Huo and B. Z. Tang, *Adv. Funct. Mater.*, 2021, **31**, 2106988.
29 P. Yin, T. Wang, Y. Yang, W. Yin, S. Zhang, Z. Yang, C. Qi and H. Ma, *New J. Chem.*, 2019, **43**, 18251–18258.

 This journal is © The Royal Society of Chemistry 2024

Open Access Article. Published on 11 April 2024. Downloaded on 2/21/2026 12:13:01 PM.
This article is licensed under a Creative Commons Attribution-NonCommercial 3.0 Unported Licence.

30 S. Xiong, Y. Xiong, D. Wang, Y. Pan, K. Chen, Z. Zhao, D. Wang and B. Z. Tang, *Adv. Mater.*, 2023, **35**, 2301874.
31 R. Geng, X. Hou, Y. Sun, C. Yan, Y. Wu, H.-L. Zhang and S. Xhao, *Mater. Chem. Front.*, 2018, **2**, 1456–1461.
32 Z. Zheng, L. Opilik, F. Schiffmann, W. Liu, G. Bergamini, P. Ceroni, L.-T. Lee, A. Schütz, J. Sakamoto, R. Zenobi, J. Vandevondele and A. D. Schlüter, *J. Am. Chem. Soc.*, 2014, **136**, 6103–6110.
33 A. Zavaleta, A. O. Lykhin, J. H. S. K. Monteiro, S. Uchida, T. W. Bell, A. De Bettencourt-Dias, S. A. Varganov and J. Gallucci, *J. Am. Chem. Soc.*, 2020, **142**, 20306–20312.
34 Z. Zhou, H. Meng, F. Li, T. Jiang, Y. Yang, S. Liu and Q. Zhao, *Inorg. Chem.*, 2023, **62**, 5729–5736.
35 H. Meng, W. Zhu, F. Li, X. Huang, Y. Qin, S. Liu, Y. Yang, W. Huang and Q. Zhao, *Laser Photonics Rev.*, 2021, **15**, 2100309.
36 X. Liu, S. Wang, W. Xie, J. Ni, K. Xiao, S. Liu, W. Lv and Q. Zhao, *J. Mater. Chem. C*, 2023, **11**, 7405–7410.
37 X. Wang, H. Shi, H. Ma, W. Ye, L. Song, J. Zan, X. Yao, X. Ou, G. Yang, Z. Zhao, M. Singh, C. Lin, H. Wang, W. Jia, Q. Wang, J. Zhi, C. Dong, X. Jiang, Y. Tang, X. Xie, Y. Yang, J. Wang, Q. Chen, Y. Wang, H. Yang, G. Zhang, Z. An, X. Liu and W. Huang, *Nat. Photonics*, 2021, **15**, 187–192.